AGU PUBLICATIONS

Geophysical Research Letters

RESEARCH LETTER
10.1002/2016GL068286

Key Points:
- Diel hydrologic fluctuations create hyporheic flow path lengths and residence times that span orders of magnitude
- Diel hydrologic fluctuations can produce hyporheic flow path residence times and lengths equivalent to those driven by geomorphic features
- Hyporheic flow path residence time and geometry are not directly coupled

Supporting Information:
- Supporting Information S1

Correspondence to:
N. M. Schmadel,
nschmadel@gmail.com

Citation:
Schmadel, N. M., A. S. Ward, C. S. Lowry, and J. M. Malzone (2016), Hyporheic exchange controlled by dynamic hydrologic boundary conditions, *Geophys. Res. Lett.*, *43*, 4408–4417, doi:10.1002/2016GL068286.

Received 15 FEB 2016
Accepted 24 APR 2016
Accepted article online 27 APR 2016
Published online 7 MAY 2016

Hyporheic exchange controlled by dynamic hydrologic boundary conditions

Noah M. Schmadel[1], Adam S. Ward[1], Christopher S. Lowry[2], and Jonathan M. Malzone[3]

[1]School of Public and Environmental Affairs, Indiana University, Bloomington, Indiana, USA, [2]Department of Geology, University at Buffalo, The State University of New York, Buffalo, New York, USA, [3]Department of Geosciences, Eastern Kentucky University, Richmond, Kentucky, USA

Abstract The relative roles of dynamic hydrologic forcing and geomorphology as controls on the timescales and magnitudes of stream-aquifer exchange and hyporheic flow paths are unknown but required for management of stream corridors. We developed a comprehensive framework relating diel hydrologic fluctuations to hyporheic exchange in the absence of geomorphic complexity. We simulated groundwater flow through an aquifer bounded by a straight stream and hillslope and under time-varying boundary conditions. We found that diel fluctuations can produce hyporheic flow path lengths and residence times that span orders of magnitude. With these results, hyporheic flow path residence times and lengths can be predicted from the timing and magnitude of diel fluctuations and valley slope. Finally, we demonstrated that dynamic hydrologic boundary conditions can produce spatial and temporal scales of hyporheic flow paths equivalent to those driven by many well-studied geomorphic features, indicating that these controls must be considered together in future efforts of upscaling to stream networks.

1. Introduction

Downstream transport of water, energy, sediment, and solutes through the stream corridor is widely conceptualized as the integration of lateral and vertical exchange between different source waters [*Harvey and Gooseff*, 2015]—such as hillslope drainage, stream water that infiltrates the riparian aquifer and returns in hyporheic flow paths, and groundwater [e.g., *Hill et al.*, 2000; *Jencso et al.*, 2010; *Lowry et al.*, 2010]. The magnitudes, timescales, locations, and timing of exchange along the stream-hyporheic-aquifer-hillslope continuum control beneficial biogeochemical and ecological processes [e.g., *Lautz and Fanelli*, 2008; *Vidon and Hill*, 2004]. However, defining and quantifying hydrologic connectivity along this continuum remains difficult due to interactions between geomorphic setting (e.g., streambed form and planform morphology) and dynamic hydrologic forcing (e.g., changes in stream discharge) [e.g., *Ward et al.*, 2012]. While some have begun to investigate the influence of these interactions on exchange [e.g., *Boano et al.*, 2013], most studies of geomorphic features (e.g., bed forms, meanders, and pool-riffle sequences) as controls on vertical and lateral exchange have been limited to steady stream discharge conditions. Considerable progress has been made in understanding streambed form [e.g., *Cardenas and Wilson*, 2007] and planform geomorphic controls on hyporheic exchange [e.g., *Cardenas*, 2009; *Gomez et al.*, 2012; *Stonedahl et al.*, 2013]. This understanding has enabled hyporheic exchange processes driven by geomorphic features to be scaled up to basins [*Gomez-Velez and Harvey*, 2014; *Gomez-Velez et al.*, 2015; *Kiel and Cardenas*, 2014]. Yet the effect of dynamic hydrologic forcing to amplify or dampen the influence of geomorphic controls remains unaccounted for in these studies. Furthermore, the possible ranges of exchange induced by dynamic hydrologic forcing alone are unknown. Consequently, the relative roles of dynamic hydrologic forcing and geomorphic controls in regulating stream-aquifer exchange are uncertain, limiting the ability to predict solute and energy transport across temporal and spatial scales.

The interaction of geomorphic and hydrologic controls can influence stream-aquifer exchange differently at a variety of temporal and spatial scales. As a first step toward representing dynamic hydrologic forcing at the seasonal scale, several studies have explored exchange alterations at different base flow conditions [*Payn et al.*, 2009; *Voltz et al.*, 2013; *Ward et al.*, 2012]. Interactions between seasonal hydrologic changes and catchment-scale geomorphic setting (e.g., topography and topology) control the spatial distribution and timing of stream-hillslope connectivity across a watershed [*Godsey and Kirchner*, 2014; *Jencso et al.*, 2009, 2010; *Larned et al.*, 2015; *McGuire and McDonnell*, 2010; *Wroblicky et al.*, 1998]. Shifts in timing and magnitudes of exchange are also controlled by interactions at smaller temporal and spatial scales. For example, while groundwater inflow can reduce the extent of bed form-induced exchange [*Boano et al.*, 2008; *Cardenas and Wilson*, 2006],

a rise in stream discharge due to a storm event can overwhelm groundwater inflow and increase the extent of exchange [*Dudley-Southern and Binley*, 2015; *Sawyer et al*., 2014a]. Increased stream discharge can also mute the influence of bed forms [*Boano et al*., 2007]. However, the interaction of dynamic hydrologic forcing and geomorphic controls associated with exchange is more likely to depend on the timing between the stream stage and aquifer water table fluctuations, potentially causing oscillating exchange patterns [*McCallum and Shanafield*, 2016; *Ward et al*., 2013; *Zimmer and Lautz*, 2014]. Similarly, diel fluctuations of stream stage can cause stream-aquifer exchange reversals. Such exchange reversals occur under a variety of hydrologic controls including snowmelt periods [e.g., *Loheide and Lundquist*, 2009], tidal cycles in estuaries [e.g., *Sawyer et al*., 2013], dam operations [e.g., *Francis et al*., 2010; *Gerecht et al*., 2011; *Sawyer et al*., 2009], and evapotranspiration [e.g., *Czikowsky and Fitzjarrald*, 2004; *Lundquist and Cayan*, 2002]. In all cases, a temporal lag occurs between stream stage and aquifer water table response. In particular, evapotranspiration is widely distributed across a watershed and expected to produce a distribution of lag times and magnitudes between the hillslope and stream [*Wondzell et al*., 2007, 2010]. Although empirical evidence of hydrologic and geomorphic controls exists, a comprehensive understanding of how dynamic timing between the stream and hillslope responses control exchange is necessary to prevent inconsistent predictions for similar types of hydrologic forcing or interactions with geomorphology.

In this study, we address the following question: how does the timing and magnitude of dynamic hydraulic gradients between the stream and hillslope, driven by diel hydrologic fluctuations, control stream-aquifer interactions? Our goal is to determine the influence of these fluctuations on hyporheic exchange flux, flow path geometry, and residence time independent of geomorphic controls. We present the results from a series of numerical simulations of groundwater flow through a straight, planar aquifer with homogeneous valley morphology under time-varying hillslope and stream boundary conditions. These results provide a framework for predicting the general responses of hyporheic flux, residence time, and extent, given the timing and magnitude of diel fluctuations. Finally, we compare the spatial and temporal scales of flow paths driven by dynamic hydrologic boundary conditions to those reported for a range of well-studied geomorphic features.

2. Methods

We constructed a two-dimensional, vertically integrated finite element model of groundwater flow through an idealized riparian aquifer bounded by the stream and hillslope (Figure 1a). The timing and magnitude of diel hillslope water table relative to the stream stage and the cross- and down-valley slopes were varied to produce a wide range of hydraulic gradients. To isolate the influence of diel hydrologic fluctuations, we considered a straight, plane-bed stream where no exchange is driven by geomorphology.

Unsteady, two-dimensional, homogeneous, horizontal, incompressible groundwater flow through the nondeformable aquifer was simulated using the Boussinesq equation,

$$\frac{\partial}{\partial x}\left(h\frac{\partial h}{\partial x}\right)+\frac{\partial}{\partial y}\left(h\frac{\partial h}{\partial y}\right)=\frac{S}{K}\frac{\partial h}{\partial t}, \tag{1}$$

where $h(x,y,t)$ is the hydraulic head (m), x is the streamwise (down-valley) direction (m), y is the cross-valley direction (m), S is the specific yield (approximated by porosity), K is the isotropic hydraulic conductivity ($\mathrm{m\,s^{-1}}$), and t is time (s). COMSOL Multiphysics was used to develop a finite element solution to equation (1) [*Li et al*., 2009]. Specific discharge was estimated using Darcy's law,

$$q_x=-K\frac{\partial h}{\partial x}, q_y=-K\frac{\partial h}{\partial y}, \tag{2}$$

where q_x and q_y are the specific discharges (i.e., Darcy fluxes) in the x and y directions ($\mathrm{m\,s^{-1}}$), respectively. The stream-aquifer boundary is sinusoidal, expressed as (Figure 1b)

$$h(x,0,t)=A_{\mathrm{st}}\sin\left(\frac{2\pi}{\omega}t\right)+Y_{\mathrm{st}}+S_x(X-x), \tag{3}$$

where ω is the period (in this case of diel fluctuations, 24 h), A_{st} is the amplitude of the stream hydraulic head fluctuation (m), Y_{st} is the stream mean hydraulic head (m), S_x is the down-valley slope, and X is the total

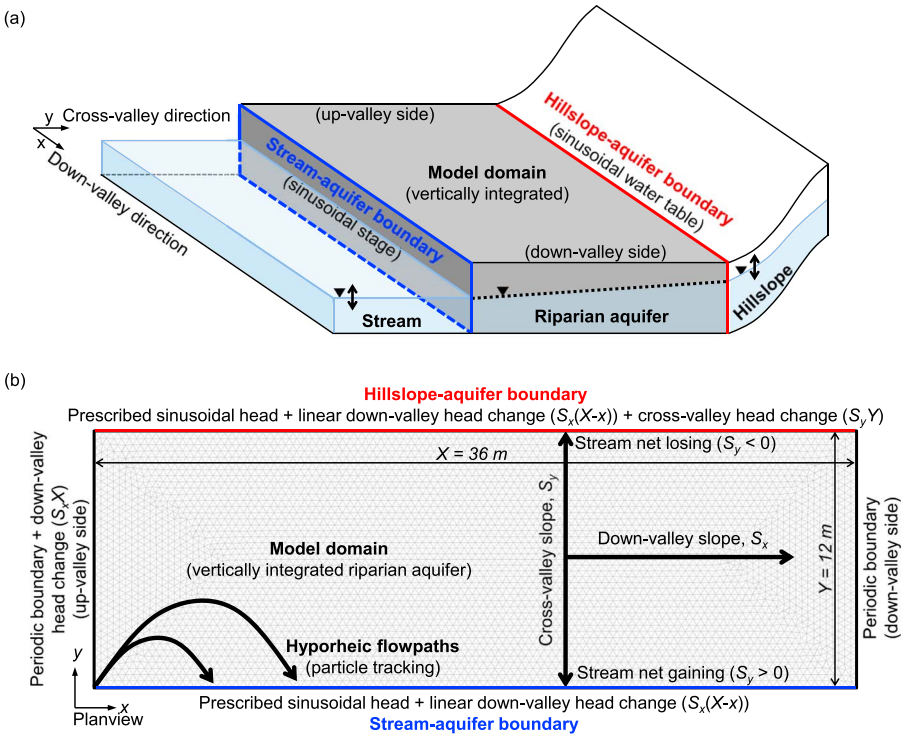

Figure 1. (a) Conceptual illustration of the model setup of groundwater flow through a vertically integrated riparian aquifer bounded by the stream and hillslope. The stage at the stream-aquifer boundary and water table at the hillslope-aquifer boundary were idealized sinusoidal diel fluctuations, producing a hydraulic gradient (see Figure S1 for examples). (b) The finite element groundwater flow model and boundary conditions in plan view where the riparian aquifer is vertically integrated. Cross-valley slope (S_y) and down-valley slope (S_x) were also varied to contribute to the hydraulic gradient. Massless particles were released at the up-valley most point of the stream-aquifer boundary and tracked to quantify hyporheic flow path residence time and length. Particles that infiltrated the aquifer and returned to the stream were considered hyporheic flow paths.

down-valley length of the model domain (m). The hillslope-aquifer boundary is also sinusoidal and includes a temporal lag, ϕ (s), relative to the stream (Figure 1b),

$$h(x,Y,t) = A_{hs}\sin\left(\frac{2\pi}{\omega}(t-\phi)\right) + Y_{hs} + S_x(X-x) + S_yY, \quad (4)$$

where A_{hs} is the amplitude of the hillslope hydraulic head fluctuation (m), Y_{hs} is the mean hydraulic head of the hillslope (m), S_y is the cross-valley slope, and Y is the total cross-valley width of the model domain (m) (see Table S1 in the supporting information for a summary of notation). The up-valley and down-valley sides (left and right sides in Figure 1b) were set to periodic boundaries to eliminate edge effects with a total head change of S_xX between them (i.e., $h(0,y,t) = S_xX$ and $h(X,y,t) = 0$) to represent a constant down-valley flow [after *Cardenas*, 2009]. These up- and down-valley boundaries are periodic only in space to approximate an infinite domain and do not vary in time. The sinusoidal components of the stream and hillslope boundary conditions are taken as uniform along the 36 m model domain, which is assumed short enough to not warrant downstream wave routing of the stream boundary condition [after *Perkins and Koussis*, 1996]. A homogeneous, isotropic hydraulic conductivity of 10^{-3} m s^{-1} was assigned to the entire model domain to eliminate the possibility of heterogeneity in the hydraulic conductivity field as a control on groundwater flow [e.g., *Salehin et al.*, 2004; *Sawyer et al.*, 2014b; *Ward et al.*, 2011]. This hydraulic conductivity value is typical for clean sand [*Freeze and Cherry*, 1979]. Based on a wide range of reported diel fluctuations, on the order of 0.01 to 1.5 m [e.g., *Francis et al.*, 2010; *Loheide and Lundquist*, 2009; *Sawyer et al.*, 2009; *Wondzell et al.*, 2010], the stream amplitude, A_{st}, was set to 0.2 m to represent a reasonably strong diel fluctuation (see Figure S1). An amplitude of this magnitude would generally coincide with large natural (e.g., evapotranspiration and snowmelt periods) and moderate anthropogenic (e.g., dam operations) fluctuations.

The hydraulic gradient in the riparian aquifer is controlled by four independent variables in this study: (1) the temporal lag in the hillslope water table relative to the stream stage (ϕ), (2) the percent amplitude of hillslope water table relative to the stream stage ($A = (A_{hs}/A_{st}) \times 100\%$) (see Figure S1 for examples), (3) the cross-valley slope (S_y), and (4) the down-valley slope (S_x) (Figure 1b). For this study, ϕ was varied from 0 to 24 h, A was varied from 0 to 100% with a fixed $A_{st} = 0.2$ m, $S_y = [-1, 0, 1]$%, and $S_x = [1, 2, 3]$%. The hillslope signal is perfectly out of phase with the stream at $\phi = 12$ h (Figure S1). Values of S_y set at -1, 0, and 1% represent net stream losing, neutral, and gaining conditions, respectively. The dynamics of the stream-hyporheic-aquifer-hillslope system were quantified by the variation of flux across the stream-aquifer boundary and by the residence times and lengths of hyporheic flow paths [after *Cardenas*, 2009]. Specifically, the maximum stream-to-aquifer flux normal to the stream-aquifer boundary was tabulated for each hydraulic gradient. Because flux is uniform along this boundary, this is represented by positive q_y (equation (2)), which is the unit flux.

Hyporheic flow path residence times and lengths were estimated through particle tracking. Massless particles were released every 5 min over one diel cycle (i.e., 24 h period) at the up-valley most point of the stream-aquifer boundary and tracked (Figure 1b). Particle velocities were estimated from the specific discharges (equation (2)) divided by a porosity of 0.30 [e.g., *Sawyer et al*., 2009; *Stonedahl et al*., 2013]. Particles that infiltrated the aquifer and returned to the stream were considered hyporheic flow paths, following common definitions [e.g., *Buffington and Tonina*, 2009; *Tonina and Buffington*, 2009; *Ward*, 2016]. The size of the model domain was selected to capture every possible hyporheic flow path for each simulated hydraulic gradient. Any particle that did not return to the stream represents either groundwater recharge or down-valley flow and was omitted from further consideration in this study. The time elapsed from particle release to return to the stream represents the hyporheic flow path residence time. To quantify flow path geometry, flow path length was separated into its components of the cross-valley (i.e., exchange penetration length into the aquifer) and down-valley lengths. Maximum residence times and lengths were tabulated for each hydraulic gradient.

3. Results

3.1. Flux Normal to the Stream-Aquifer Boundary

The magnitude of flux normal to the stream-aquifer boundary was primarily controlled by the hillslope lag (ϕ) and amplitude (A) while cross-valley slope (S_y) controlled the relative amounts of stream net gaining or losing (Figure 2). The largest stream-to-aquifer flux occurred at $\phi = 12$ h, $A = 100$%, and $S_y = -1$% (Figure 2 a, left column), which produced the largest hydraulic gradient between the stream- and hillslope-aquifer boundaries. As ϕ was shifted from 0 to 12 h (x axes in Figure 2a), the diel hillslope signal became increasingly out of phase with the stream signal and, consequently, increased the magnitude of stream-to-aquifer flux (Figure 2a). Likewise, as ϕ was shifted from 12 to 24 h, the diel signals became increasingly in phase, thus reducing the hydraulic gradient between the stream and hillslope and, in turn, reducing the magnitude of stream-to-aquifer flux. As S_y was varied from -1 to 1%, the maximum stream-to-aquifer flux possible within one diel cycle generally decreased (Figure 2a, left-to-right columns). A S_y of -1% created a larger hydraulic gradient toward the hillslope over one diel cycle and, therefore, produced a net losing stream. Conversely, a S_y of 1% created hydraulic gradients that opposed stream-to-aquifer flux and produced a net gaining stream. An increase in down-valley slope (S_x) from 1 to 3% did not change the magnitude of flux (Figure 2 a, top-to-bottom rows). While stream-to-aquifer flux was insensitive to S_x for this study, it was controlled by ϕ, A, and S_y (Figure 2).

In addition to the maximum stream-to-aquifer fluxes tabulated for each hydraulic gradient (Figure 2a), the diel variation in flux across the stream-aquifer boundary changed in response to the boundary conditions (Figures 2b–2e). The model simulations shown in these panels were selected to demonstrate how ϕ, A, S_y, and S_x individually control the timing and variability of flux. When ϕ was varied from 0 to 12 h (fixed $A = 100$%, $S_y = 1$%, and $S_x = 3$%), the magnitude and time of peak flux systematically increased (Figure 2b where maxima and colors correspond to the bottom right panel of Figure 2a). For example, when ϕ was 12 h (see light green line in Figure 2b), the maximum occurred at 6 h (minimum at 18 h). A change in S_y from -1 to 1% (fixed $A = 100$%, $\phi = 12$ h, and $S_x = 3$%) primarily affected the relative magnitudes of aquifer-to-stream and stream-to-aquifer flux, which had a slight influence on the timing of flux direction (Figure 2c where maxima and colors

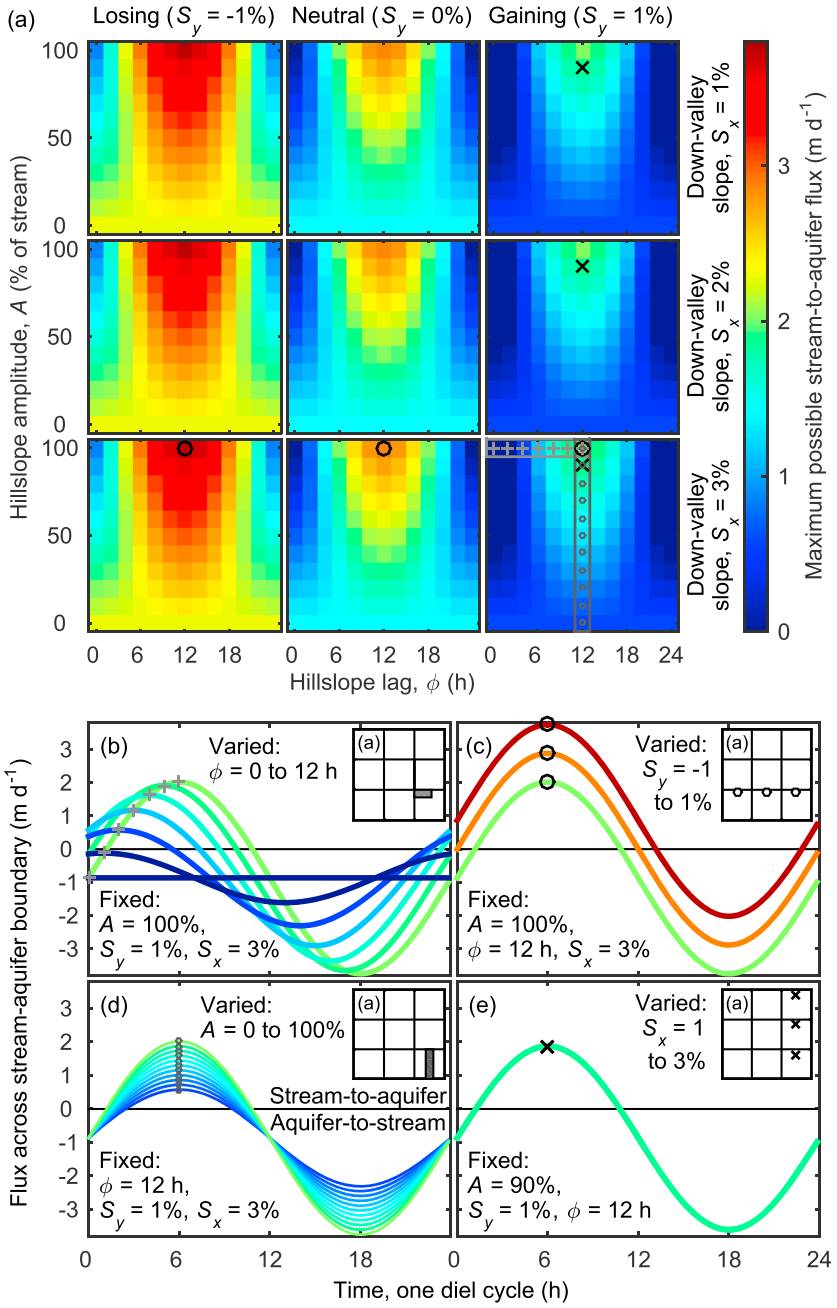

Figure 2. Darcy flux of water across (normal to) the stream-aquifer boundary (q_y) for varying hillslope lag (ϕ), percent hillslope amplitude relative to the stream (A), cross-valley slope (S_y), and down-valley slope (S_x). (a) Summary results of the maximum possible stream-to-aquifer flux across the stream-aquifer boundary for each combination of ϕ (x axis) and A (y axis) under different S_y (left-to-right columns) and S_x (top-to-bottom rows). The symbols in Figure 2a correspond to the example time series of flux in Figures 2b–2e, selected to demonstrate how ϕ, A, S_y, and S_x individually control the timing and variability of flux in addition to the maximum stream-to-aquifer fluxes. Line colors in Figures 2b–2e correspond to maxima (and symbols) in Figure 2a where inset legends indicate locations in Figures 2a. (b) ϕ was varied while A, S_y, and S_x, were fixed. (c) S_y was varied while A, ϕ, and S_x were fixed. (d) A was varied while ϕ, S_y, and S_x were fixed. (e) S_x was varied while A, S_y, and ϕ were fixed.

correspond to the black circles in the bottom row of Figure 2a). Subsequently, when $S_y = 1\%$ (cross-valley slope toward the stream), the stream-to-aquifer flux was lowest and aquifer-to-stream flux was greatest, which resulted in a net gaining stream (Figure 2c). A change in A from 0 to 100% (fixed $\phi = 12$ h, $S_y = 1\%$, and $S_x = 3\%$) primarily affected the magnitude of stream-to-aquifer flux (Figure 2d where maxima and colors correspond

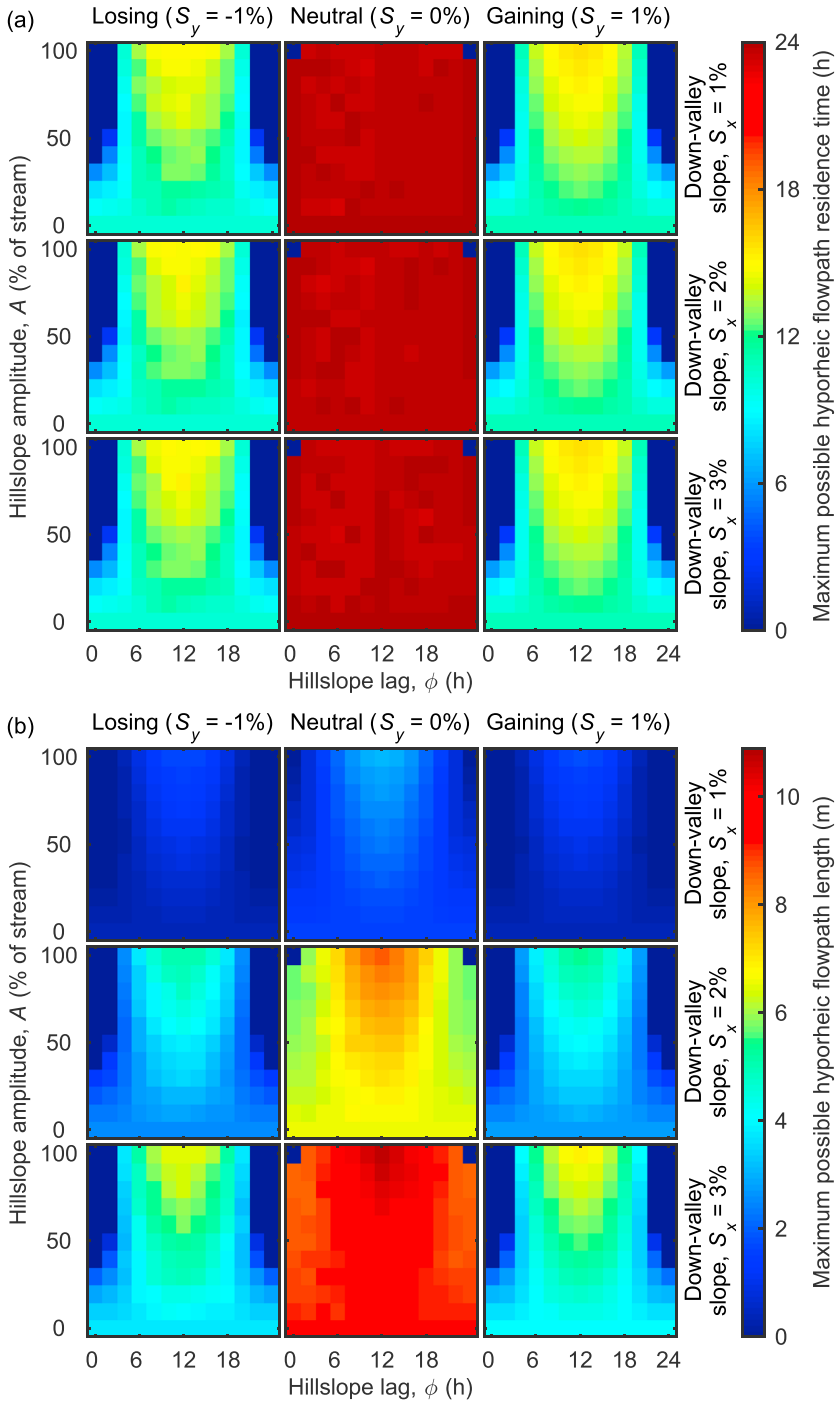

Figure 3. Hyporheic flow path residence time and length for varying hillslope lag (ϕ), percent hillslope amplitude relative to the stream (A), cross-valley slope (S_y), and down-valley slope (S_x). (a) Summary results of the maximum possible hyporheic flow path residence time for each combination of ϕ, A, S_y, and S_x. (b) Summary results of the maximum possible hyporheic flow path length for each combination of ϕ, A, S_y, and S_x.

to the bottom right panel of Figure 2a). Net flux was primarily controlled by S_y. Varying S_x from 1 to 3% (fixed $A = 90\%$, $S_y = 1\%$, and $\phi = 12$ h) had no effect on flux normal to the stream-aquifer boundary (Figure 2e where maxima and colors correspond to the black crosses in the right column of Figure 2a). In summary, ϕ primarily controlled the timing of the exchange flux while S_y determined net gaining or losing conditions. The magnitude of the flux was controlled by ϕ, A, and S_y; S_x had no effect on flux.

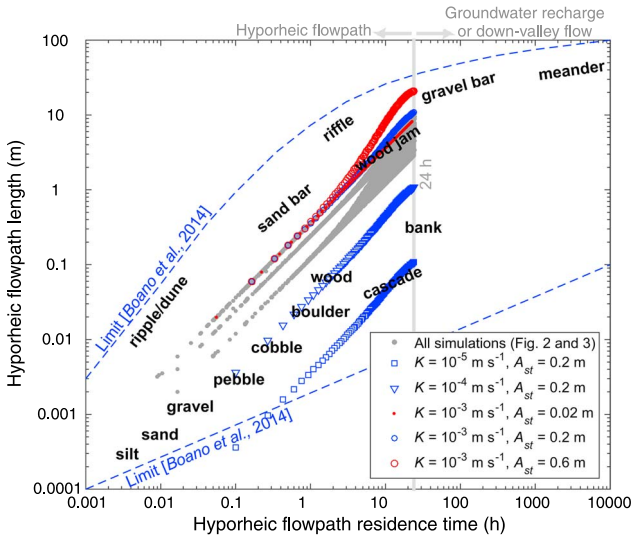

Figure 4. Hyporheic flow path residence times and lengths induced by diel hydrologic fluctuations compared to those induced by general geomorphic features synthesized by *Boano et al.* [2014]. Results of all the simulations in this manuscript (see Figures 2 and 3) are shown in gray circles where an isotropic hydraulic conductivity (K) of 10^{-3} m s^{-1} was used. To define the plausible range of hyporheic flow paths induced by diel fluctuations, additional simulations were run varying K between 10^{-5} and 10^{-3} m s^{-1} and stream amplitude (A_{st}) between 0.02 and 0.6 m (fixing hillslope lag at 12 h, percent hillslope amplitude relative to the stream at 100%, cross-valley slope at 0%, and down-valley slope at 3%). The vertical gray line at 24 h is the maximum possible flow path residence time induced by diel fluctuations. The blue dashed lines represent the limits of hyporheic flow paths, and bold text represents general flow path residence times and lengths induced by geomorphic features, which were reproduced from *Boano et al.* [2014]. Note that Boano et al. scaled the y axis as hyporheic dimension/channel width. Here hyporheic flow path length is based on a unit channel width.

3.2. Hyporheic Flow Path Residence Time and Length

The maximum hyporheic flow path residence time possible over one diel cycle was primarily controlled by S_y (Figure 3a). The magnitude of residence time was sensitive to ϕ and A only when S_y was less than or greater than zero (nonneutral conditions, Figure 3a, left and right columns). Otherwise, when the cross-valley slope did not contribute to the overall hydraulic gradient, the magnitude of residence time was insensitive to ϕ and A and set solely by the sinusoidal, 24 h period of hillslope and stream fluctuations (Figure 3a, middle column). Under this neutral condition, with the exception of $\phi = 0$ or 24 h (in phase) and $A = 100\%$ where the stream and hillslope signals together produced no hydraulic gradient, any particle that infiltrated the aquifer was driven back into the stream within 24 h (uniform maxima of 24 h shown in Figure 3a, middle column; see Figure S2 for residence times as a function of particle release time). The corresponding mean residence times (not shown) followed the same pattern as in Figure 3a, indicating that these maxima reflect the primary controls on residence time. In summary, the hyporheic flow path residence time was controlled by ϕ and A under nonneutral conditions and insensitive to ϕ and A under neutral conditions. Flow path residence time was always sensitive to S_y and insensitive to S_x.

While residence time was controlled by ϕ and A under nonneutral conditions ($S_y \neq 0\%$) and insensitive to S_x, hyporheic flow path length was sensitive to ϕ, A, S_y, and S_x for each hydraulic gradient (Figure 3b). For example, under neutral conditions ($S_y = 0\%$), the maximum flow path length possible over one diel cycle increased as ϕ was shifted from 0 to 12 h and as A was increased from 0 to 100% (Figure 3b, middle column). Furthermore, a change in S_x from 1 to 3% increased the flow path length (Figure 3b, top-to-bottom rows). A key finding is that different hyporheic flow path lengths induced by the same hydrologic forcing can have identical residence times. Therefore, flow path residence time and geometry are not directly coupled. In terms of flow path geometry, the cross-valley component of length was primary controlled by ϕ, A, and S_y and insensitive to S_x (see Figure S3). Conversely, the down-valley component of length was primarily controlled by S_x (see Figure S4). In summary, hyporheic flow path length was always controlled by ϕ, A, S_y, and S_x; however, the cross-valley component was always insensitive to S_x. See Figure S5 for a synthesis of how ϕ, A, S_y, and S_x control stream-to-aquifer flux and hyporheic flow path residence time and length.

4. Discussion

4.1. Diel Hydrologic Fluctuations and Geomorphic Controls Can Produce Equivalent Hyporheic Flow Path Residence Times and Lengths

Based on our simulations, diel hydrologic fluctuations can produce hyporheic flow paths that span more than 3 orders of magnitude in spatial and temporal scales (Figure 4). These spatial and temporal scales are

equivalent to those produced by many geomorphic features synthesized by *Boano et al.* [2014] (and by *Harvey and Wagner* [2000], Figure S6). To further define the plausible range of hyporheic flow paths induced by diel fluctuations, we ran additional simulations varying hydraulic conductivity (K) across 3 orders of magnitude (fixing $\phi = 12$ h, $A = 100\%$, $S_y = 0\%$, and $S_x = 3\%$, which were shown to produce the longest possible hyporheic flow paths). Overall, a larger K resulted in longer hyporheic flow paths, though residence times remained unchanged, further demonstrating that flow paths of different lengths can have identical residence times. Simulated flow paths lower than the limit of hyporheic exchange synthesized by *Boano et al.* [2014] had long residence times relative to extremely small lengths. While model simulations may capture flow paths at such small spatial scales, it is unlikely that these would be reflected in field-based measurements. We also varied stream amplitude from 0.02 to 0.6 m (again fixing $\phi = 12$ h, $A = 100\%$, $S_y = 0\%$, and $S_x = 3\%$ and holding $K = 10^{-3}$ m s^{-1}). An increased stream amplitude caused longer flow path lengths and residence times. However, even small diel fluctuations (e.g., 0.02 m stream amplitude) produced residence times up to 24 h; any residence time longer than this became down-valley flow or groundwater recharge in our simulated system (right of the vertical gray line in Figure 4). If the hillslope amplitude becomes greater than the stream (i.e., $A > 100\%$), magnitudes of cross-valley hydraulic gradients increase. As a result, peak exchange flux and hyporheic flow path mean residence times and lengths (including the cross- and down-valley components) all increase but follow the same patterns as in Figures 2 and 3. The net flux over one diel cycle and maximum possible residence time of 24 h, however, remain unchanged. This temporal threshold is set by the idealized sinusoidal fluctuations and subsurface homogeneity and, therefore, emphasizes a need to consider additional constraints of subsurface heterogeneity [e.g., *Sawyer et al.*, 2014b], stream morphology in profile or planform [e.g., *Boano et al.*, 2014; *Gomez-Velez and Harvey*, 2014], changes in valley width or depth with stream order [e.g., *Kasahara and Wondzell*, 2003; *Wondzell and Swanson*, 1999], and deviation from the idealized sinusoidal forcing [e.g., *Wondzell et al.*, 2007, 2010]. In practice, we expect that any such complexity introduced would extend hyporheic flow path residence times beyond 24 h.

Another aspect to consider is the relative effect of shorter-term to longer-term hydrologic fluctuations on hyporheic exchange. For example, the stream stage may respond to shorter-term hydrologic controls (e.g., evapotranspiration or storm events), while the hillslope water table responds to longer-term (e.g., seasonal) controls. In the case of a rapidly varied stream (e.g., 24 h frequency) and a much longer wavelength hillslope fluctuation (e.g., annual cycle), the hillslope water table is functionally static ($A \approx 0\%$) over the timescale of an individual cycle of the stream-aquifer boundary. As such, our $A = 0\%$ results are reasonable approximations of systems where stream and hillslope fluctuations occur over very different timescales. Subsequently, a change in hillslope water table through the season can be approximated similarly to our change in cross-valley slope. Appropriately representing longer-term hillslope fluctuations may be important as these can control stream-hillslope connectivity and riparian aquifer turnover [e.g., *Godsey and Kirchner*, 2014; *Jencso et al.*, 2010]. Our results, however, clearly show the range of hyporheic residence times, exchange fluxes, and flow path lengths arising from diel hydrologic fluctuations. Furthermore, these results form the basis required to transfer reach-scale findings to network-scale predictions, as in *Kiel and Cardenas* [2014] and *Gomez-Velez et al.* [2015].

4.2. Existing Anthropogenic Control of Diel Fluctuations Could Be Leveraged to Achieve Beneficial Outcomes

In regulated rivers, stage fluctuations can occur due to hydropower generation, wastewater discharge, or irrigation withdrawals. The framework developed in this study to anticipate hyporheic flow path residence times and extent from the timing and magnitude of diel fluctuations could be leveraged as a river management tool. While down- and cross-valley slopes generally cannot be controlled, stream stage and riparian aquifer fluctuations characterized by amplitudes and temporal lags (phase shifts) are within the realm of human control in certain settings. Based on our results, to achieve minimal exchange, the timing and magnitude of stream stage fluctuations would need to coincide with the timing and magnitude of the hillslope water table (i.e., in phase; Figure 2). Conversely, to achieve maximum exchange, stream stage would need to be out of phase with the hillslope. When these signals are out of phase, larger amplitudes in the stream and hillslope generate larger magnitudes of exchange and hyporheic flow path residence times and lengths (Figures 2 and 3).

This type of coupled surface and subsurface flow response could be considered as part of the design of non-emergency flow releases for dams and possibly as a mitigation measure as part of dam relicensure. For example, by controlling the timing of stream stage fluctuations relative to aquifer withdrawals, such as riverbank filtration

for drinking water or irrigation withdrawals downstream of a hydropower dam, a manager could manipulate hyporheic exchange to achieve timescales that would enable desirable functions (e.g., denitrification [e.g., *Harvey et al*., 2013; *Rahimi et al*., 2015] or creation of thermal refugia for fish [e.g., *Bowerman et al*., 2014; *Mathes et al*., 2009]). Alternatively, exchange could be intentionally reduced to provide environmental benefits. Consider a contaminant plume near a stream, where remediation action could include pumping designed to offset stream fluctuations and reduce connectivity of the stream to that potential contaminant source. Improved water resource management across temporal (e.g., daily to seasonal) and spatial (e.g., feature to basin) scales will require dynamic hydrologic studies over more heterogeneous forcing events (e.g., snowmelt and storms) and simultaneous consideration of interactions with geomorphic controls. This study provides a necessary foundation to introduce such complexities in future studies.

Acknowledgments

Schmadel and Ward were supported in part by the National Science Foundation grant EAR 1331906 for the Critical Zone Observatory for Intensively Managed Landscapes (IML-CZO), a multi-institutional collaborative effort, by NSF grant EAR 1505309, by the U.S. Department of Agriculture (USDA) grant 2013-67019-21365, by the Indiana University Office of the Vice Provost for Research, and by the Indiana Water Resources Research Center. Any opinions, findings, conclusions, or recommendations expressed here are those of the authors and do not necessarily represent the official views of sponsoring agencies. The authors thank the Editors, one anonymous reviewer, and Susa Stonedahl for their thoughtful comments to improve this manuscript. Flux and particle tracking data are available upon request to the corresponding author. The authors declare no conflicts of interest.

References

Boano, F., R. Revelli, and L. Ridolfi (2007), Bedform-induced hyporheic exchange with unsteady flows, *Adv. Water Resour.*, *30*(1), 148–156.

Boano, F., R. Revelli, and L. Ridolfi (2008), Reduction of the hyporheic zone volume due to the stream-aquifer interaction, *Geophys. Res. Lett.*, *35*, L09401, doi:10.1029/2008GL033554.

Boano, F., R. Revelli, and L. Ridolfi (2013), Modeling hyporheic exchange with unsteady stream discharge and bedform dynamics, *Water Resour. Res.*, *49*, 4089–4099, doi:10.1002/wrcr.20322.

Boano, F., J. W. Harvey, A. Marion, A. I. Packman, R. Revelli, L. Ridolfi, and A. Wörman (2014), Hyporheic flow and transport processes: Mechanisms, models, and biogeochemical implications, *Rev. Geophys.*, *52*, 603–679, doi:10.1002/2012RG000417.

Bowerman, T., B. T. Neilson, and P. Budy (2014), Effects of fine sediment, hyporheic flow, and spawning site characteristics on survival and development of bull trout embryos, *Can. J. Fish. Aquat. Sci.*, *71*(7), 1059–1071.

Buffington, J. M., and D. Tonina (2009), Hyporheic exchange in mountain rivers. II: Effects of channel morphology on mechanics, scales, and rates of exchange, *Geogr. Compass*, *3*(3), 1038–1062.

Cardenas, M. B. (2009), Stream-aquifer interactions and hyporheic exchange in gaining and losing sinuous streams, *Water Resour. Res.*, *45*, W06429, doi:10.1029/2008WR007651.

Cardenas, M. B., and J. L. Wilson (2006), The influence of ambient groundwater discharge on exchange zones induced by current–bedform interactions, *J. Hydrol.*, *331*(1–2), 103–109.

Cardenas, M. B., and J. L. Wilson (2007), Hydrodynamics of coupled flow above and below a sediment–water interface with triangular bedforms, *Adv. Water Resour.*, *30*(3), 301–313.

Czikowsky, M. J., and D. R. Fitzjarrald (2004), Evidence of seasonal changes in evapotranspiration in eastern U.S. hydrological records, *J. Hydrometeorol.*, *5*(5), 974–988.

Dudley-Southern, M., and A. Binley (2015), Temporal responses of groundwater-surface water exchange to successive storm events, *Water Resour. Res.*, *51*, 1112–1126, doi:10.1002/2014WR016623.

Francis, B. A., L. K. Francis, and M. B. Cardenas (2010), Water table dynamics and groundwater–surface water interaction during filling and draining of a large fluvial island due to dam-induced river stage fluctuations, *Water Resour. Res.*, *46*, W07513, doi:10.1029/2009WR008694.

Freeze, R. A., and J. A. Cherry (1979), *Groundwater*, Prentice Hall, Engelwood Cliffs, N. J.

Gerecht, K. E., M. B. Cardenas, A. J. Guswa, A. H. Sawyer, J. D. Nowinski, and T. E. Swanson (2011), Dynamics of hyporheic flow and heat transport across a bed-to-bank continuum in a large regulated river, *Water Resour. Res.*, *47*, W03524, doi:10.1029/2010WR009794.

Godsey, S. E., and J. W. Kirchner (2014), Dynamic, discontinuous stream networks: Hydrologically driven variations in active drainage density, flowing channels and stream order, *Hydrol. Processes*, *28*(23), 5791–5803.

Gomez, J. D., J. L. Wilson, and M. B. Cardenas (2012), Residence time distributions in sinuosity-driven hyporheic zones and their biogeochemical effects, *Water Resour. Res.*, *48*, W09533, doi:10.1029/2012WR012180.

Gomez-Velez, J. D., and J. W. Harvey (2014), A hydrogeomorphic river network model predicts where and why hyporheic exchange is important in large basins, *Geophys. Res. Lett.*, *41*, 6403–6412, doi:10.1002/2014GL061099.

Gomez-Velez, J. D., J. W. Harvey, M. B. Cardenas, and B. Kiel (2015), Denitrification in the Mississippi River network controlled by flow through river bedforms, *Nat. Geosci.*, *8*(12), 941–945.

Harvey, J., and M. Gooseff (2015), River corridor science: Hydrologic exchange and ecological consequences from bedforms to basins, *Water Resour. Res.*, *51*, 6893–6922, doi:10.1002/2015WR017617.

Harvey, J. W., and B. J. Wagner (2000), Quantifying hydrologic interactions between streams and their subsurface zones, in *Streams and Ground Waters*, edited by J. B. Jones and P. J. Mulholland, pp. 3–44, Academic Press, San Diego, Calif.

Harvey, J. W., J. K. Böhlke, M. A. Voytek, D. Scott, and C. R. Tobias (2013), Hyporheic zone denitrification: Controls on effective reaction depth and contribution to whole-stream mass balance, *Water Resour. Res.*, *49*, 6298–6316, doi:10.1002/wrcr.20492.

Hill, A. R., K. J. Devito, S. Campagnolo, and K. Sanmugadas (2000), Subsurface denitrification in a forest riparian zone: Interactions between hydrology and supplies of nitrate and organic carbon, *Biogeochemistry*, *51*(2), 193–223.

Jencso, K. G., B. L. McGlynn, M. N. Gooseff, S. M. Wondzell, K. E. Bencala, and L. A. Marshall (2009), Hydrologic connectivity between landscapes and streams: Transferring reach- and plot-scale understanding to the catchment scale, *Water Resour. Res.*, *45*, W04428, doi:10.1029/2008WR007225.

Jencso, K. G., B. L. McGlynn, M. N. Gooseff, K. E. Bencala, and S. M. Wondzell (2010), Hillslope hydrologic connectivity controls riparian groundwater turnover: Implications of catchment structure for riparian buffering and stream water sources, *Water Resour. Res.*, *46*, W10524, doi:10.1029/2009WR008818.

Kasahara, T., and S. M. Wondzell (2003), Geomorphic controls on hyporheic exchange flow in mountain streams, *Water Resour. Res.*, *39*(1), 1005, doi:10.1029/2002WR001386.

Kiel, B. A., and M. B. Cardenas (2014), Lateral hyporheic exchange throughout the Mississippi River network, *Nat. Geosci.*, *7*(6), 413–417.

Larned, S. T., M. J. Unwin, and N. C. Boustead (2015), Ecological dynamics in the riverine aquifers of a gaining and losing river, *Freshwat. Sci.*, *34*(1), 245–262.

Lautz, L. K., and R. M. Fanelli (2008), Seasonal biogeochemical hotspots in the streambed around restoration structures, *Biogeochemistry*, *91*(1), 85–104.

Li, Q., K. Ito, Z. Wu, C. S. Lowry, and S. P. Loheide Ii (2009), COMSOL Multiphysics: A novel approach to ground water modeling, *Ground Water*, *47*(4), 480–487.
Loheide, S. P., and J. D. Lundquist (2009), Snowmelt-induced diel fluxes through the hyporheic zone, *Water Resour. Res.*, *45*, W07404, doi:10.1029/2008WR007329.
Lowry, C. S., J. S. Deems, S. P. Loheide Ii, and J. D. Lundquist (2010), Linking snowmelt-derived fluxes and groundwater flow in a high elevation meadow system, Sierra Nevada Mountains, California, *Hydrol. Processes*, *24*(20), 2821–2833.
Lundquist, J. D., and D. R. Cayan (2002), Seasonal and spatial patterns in diurnal cycles in streamflow in the western United States, *J. Hydrometeorol.*, *3*(5), 591–603.
Mathes, M. T., S. G. Hinch, S. J. Cooke, G. T. Crossin, D. A. Patterson, A. G. Lotto, and A. P. Farrell (2009), Effect of water temperature, timing, physiological condition, and lake thermal refugia on migrating adult Weaver Creek sockeye salmon (Oncorhynchus nerka), *Can. J. Fish. Aquat. Sci.*, *67*(1), 70–84.
McCallum, J. L., and M. Shanafield (2016), Residence times of stream-groundwater exchanges due to transient stream stage fluctuations, *Water Resour. Res.*, *52*, 2059–2073, doi:10.1002/2015WR017441.
McGuire, K. J., and J. J. McDonnell (2010), Hydrological connectivity of hillslopes and streams: Characteristic time scales and nonlinearities, *Water Resour. Res.*, *46*, W10543, doi:10.1029/2010WR009341.
Payn, R. A., M. N. Gooseff, B. L. McGlynn, K. E. Bencala, and S. M. Wondzell (2009), Channel water balance and exchange with subsurface flow along a mountain headwater stream in Montana, United States, *Water Resour. Res.*, *45*, W11427, doi:10.1029/2008WR007644.
Perkins, S. P., and A. D. Koussis (1996), Stream-aquifer interaction model with diffusive wave routing, *J. Hydraul. Eng.*, *122*(4), 210.
Rahimi, M., H. I. Essaid, and J. T. Wilson (2015), The role of dynamic surface water-groundwater exchange on streambed denitrification in a first-order, low-relief agricultural watershed, *Water Resour. Res.*, *51*, 9514–9538, doi:10.1002/2014WR016739.
Salehin, M., A. I. Packman, and M. Paradis (2004), Hyporheic exchange with heterogeneous streambeds: Laboratory experiments and modeling, *Water Resour. Res.*, *40*, W11504, doi:10.1029/2003WR002567.
Sawyer, A. H., M. Bayani Cardenas, A. Bomar, and M. Mackey (2009), Impact of dam operations on hyporheic exchange in the riparian zone of a regulated river, *Hydrol. Processes*, *23*(15), 2129–2137.
Sawyer, A. H., F. Shi, J. T. Kirby, and H. A. Michael (2013), Dynamic response of surface water-groundwater exchange to currents, tides, and waves in a shallow estuary, *J. Geophys. Res. Oceans*, *118*, 1749–1758, doi:10.1002/jgrc.20154.
Sawyer, A. H., L. A. Kaplan, O. Lazareva, and H. A. Michael (2014a), Hydrologic dynamics and geochemical responses within a floodplain aquifer and hyporheic zone during Hurricane Sandy, *Water Resour. Res.*, *50*, 4877–4892, doi:10.1002/2013WR015101.
Sawyer, A. H., O. Lazareva, K. D. Kroeger, K. Crespo, C. S. Chan, T. Stieglitz, and H. A. Michael (2014b), Stratigraphic controls on fluid and solute fluxes across the sediment-water interface of an estuary, *Limnol. Oceanogr.*, *59*(3), 997–1010.
Stonedahl, S. H., J. W. Harvey, and A. I. Packman (2013), Interactions between hyporheic flow produced by stream meanders, bars, and dunes, *Water Resour. Res.*, *49*, 5450–5461, doi:10.1002/wrcr.20400.
Tonina, D., and J. M. Buffington (2009), Hyporheic exchange in mountain rivers. I: Mechanics and environmental effects, *Geogr. Compass*, *3*(3), 1063–1086.
Vidon, P. G. F., and A. R. Hill (2004), Landscape controls on nitrate removal in stream riparian zones, *Water Resour. Res.*, *40*, W03201, doi:10.1029/2003WR002473.
Voltz, T., M. Gooseff, A. S. Ward, K. Singha, M. Fitzgerald, and T. Wagener (2013), Riparian hydraulic gradient and stream-groundwater exchange dynamics in steep headwater valleys, *J. Geophys. Res. Earth Surface*, *118*, 953–969, doi:10.1002/jgrf.20074.
Ward, A. S. (2016), The evolution and state of interdisciplinary hyporheic research, *Wiley Interdiscip. Rev. Water*, *3*(1), 83–103.
Ward, A. S., M. N. Gooseff, and P. A. Johnson (2011), How can subsurface modifications to hydraulic conductivity be designed as stream restoration structures? Analysis of Vaux's conceptual models to enhance hyporheic exchange, *Water Resour. Res.*, *47*, W08512, doi:10.1029/2010WR010028.
Ward, A. S., M. Fitzgerald, M. N. Gooseff, T. J. Voltz, A. M. Binley, and K. Singha (2012), Hydrologic and geomorphic controls on hyporheic exchange during base flow recession in a headwater mountain stream, *Water Resour. Res.*, *48*, W04513, doi:10.1029/2011WR011461.
Ward, A. S., M. N. Gooseff, T. J. Voltz, M. Fitzgerald, K. Singha, and J. P. Zarnetske (2013), How does rapidly changing discharge during storm events affect transient storage and channel water balance in a headwater mountain stream?, *Water Resour. Res.*, *49*, 5473–5486, doi:10.1002/wrcr.20434.
Wondzell, S. M., and F. J. Swanson (1999), Floods, channel change, and the hyporheic zone, *Water Resour. Res.*, *35*(2), 555–567, doi:10.1029/1998WR900047.
Wondzell, S. M., M. N. Gooseff, and B. L. McGlynn (2007), Flow velocity and the hydrologic behavior of streams during baseflow, *Geophys. Res. Lett.*, *34*, L24404, doi:10.1029/2007GL031256.
Wondzell, S. M., M. N. Gooseff, and B. L. McGlynn (2010), An analysis of alternative conceptual models relating hyporheic exchange flow to diel fluctuations in discharge during baseflow recession, *Hydrol. Processes*, *24*(6), 686–694.
Wroblicky, G. J., M. E. Campana, H. M. Valett, and C. N. Dahm (1998), Seasonal variation in surface-subsurface water exchange and lateral hyporheic area of two stream-aquifer systems, *Water Resour. Res.*, *34*(3), 317–328, doi:10.1029/97WR03285.
Zimmer, M. A., and L. K. Lautz (2014), Temporal and spatial response of hyporheic zone geochemistry to a storm event, *Hydrol. Processes*, *28*(4), 2324–2337.